Conference paper

Anna A. Semenova, Irina A. Veselova, Nadezhda A. Brazhe, Andrei V. Shevelkov and Eugene A. Goodilin*

Soft chemistry of pure silver as unique plasmonic metal of the Periodic Table of Elements

https://doi.org/10.1515/pac-2020-0104

Abstract: The International Year of The Periodic Table of Chemical Elements revealed that the Table remains both a deeply fundamental paradigm for various branches of chemistry and a universal practical tool for predictable design of new materials. Silver is a notable "nanoelement" particularly known by its plasmonic properties. A key advantage of this metal is an easily achievable morphological variety of nanostructured materials. This element represents a research branch of precise engineering of shapes and sizes of nanoparticle ensembles and smart hierarchic nanostructures. In the review, unique features of silver are discussed with respect to the development of novel analytical methods for forthcoming applications of surface-enhanced Raman spectroscopy (SERS) in ecology, biology and medicine.

Keywords: medical diagnostics; Mendeleev-21; nanomaterials; nanoparticles; nanotechnology; Periodic Table of Elements; SERS; silver; surface-enhanced Raman spectroscopy.

Introduction

The International Year of the Periodic Table of Chemical Elements has recalled the high importance of the Periodic Table for chemistry, modern sciences and, especially, as a powerful tool for design of advanced materials [1–11]. Nanotechnologies bring a new insight into this most important discovery [2, 4, 9]. Fig. 1 demonstrates a 3D representation of nanotechnological popularity of the elements. Most of the elements are widely spread and cheap light elements with reasonable biocompatibility, or chemically inert elements, or the elements with special redox and crystal chemistry involved in revolutionary applications in the fields of electrochemical, hydrogen and solar energy, traditional, electro- and photocatalysis, theranostics and medicine, optical, magnetic recording, informational technologies and electronics, novel construction materials [12–27]. Chemistry enables effective combinations of different elements into nanoscale structures with increased complexity to achieve new properties. By this, nanotechnologies use the best chemical features of the elements for nanoscale engineering of innovative devices.

Silver and gold are notable "nanoelements", known particularly for their plasmonic properties and related applications. A key advantage of these metals is a morphological variety of nanostructured materials. Thus the

Article note: A collection of invited papers based on presentations at the 21st Mendeleev Congress on General and Applied Chemistry (Mendeleev-21), held in Saint Petersburg, Russian Federation, 9–13 September 2019.

***Corresponding author: Eugene A. Goodilin**, Department of Materials Science and Department of Chemistry, Lomonosov Moscow State University, Moscow, 119991, Russia, e-mail: goodilin@inorg.chem.msu.ru
Anna A. Semenova: Department of Materials Science, Lomonosov Moscow State University, Moscow, 119991, Russia
Irina A. Veselova and Andrei V. Shevelkov: Department of Chemistry, Lomonosov Moscow State University, Moscow, 119991, Russia
Nadezhda A. Brazhe: Department of Biology, Lomonosov Moscow State University, Moscow, 119991, Russia

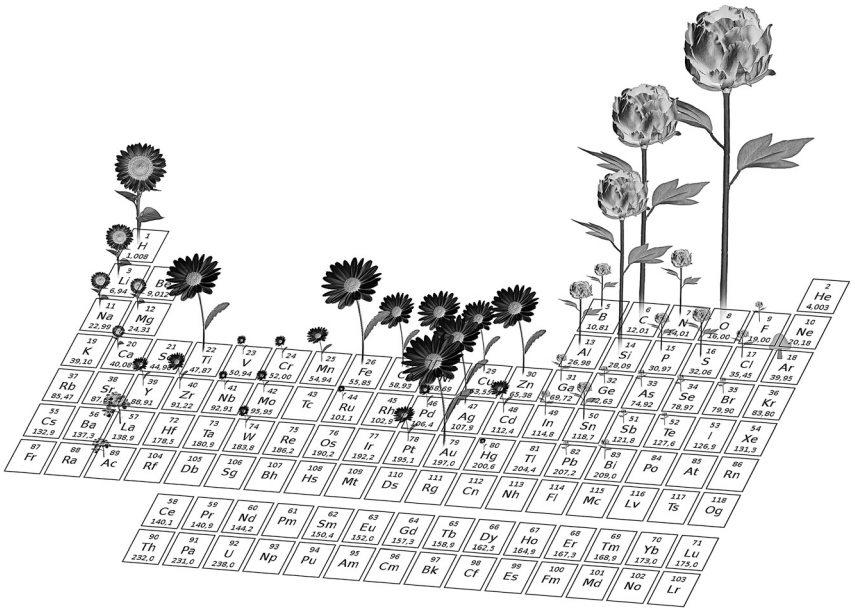

Fig. 1: Art representation of nanotechnological popularity of elements of the Periodic Table of Elements. Sunflowers, peony, daisy, forget-me-not flowers correspond to first letters of the, s-, p-, d-, f-blocks (adopted from [9]).

elements represent a special research branch dedicated to precise engineering of shapes and sizes of nanoparticles by facile methods including kinetically controlled, aggregation-based, heterogeneously seeded, template-directed growth. These most popular procedures, as a rule, are well established and result in highly controlled complex morphologies like nanoflowers, nanorices, cubs, multipods and nanodendrites, mesocages, they allow the creation of nanoparticle ensembles and "smart" hierarchic nanostructures [28–45]; in addition, gold plays a great role in self-assembly, soft lithography and photothermal therapy [46–48].

Modern noninvasive medical diagnostics for screening and personal medicine provides the challenge of highly sensitive single molecule or single cell analysis and thus demands the thorough development of innovative materials and novel analytical approaches. In this context, Raman scattering spectroscopy (RSS) is especially suited for the detection of fingerprints of various molecules, viruses, DNA, biomolecule conformations and interactions in biological samples, even in living cells, by reason of a negligible influence of fluorescence and interference from water. However, natural concentrations of enzymes, structural and signaling molecules in living cells are usually much lower than the detection limit of conventional RSS. Surface-enhanced Raman spectroscopy (SERS), for which silver nanostructures have proven to be a common choice due to a broad plasmon resonance, high stability and facile fabrication methods, solves this problem since the signal can be 10^{10}–10^{14}-fold enhanced for model molecules; this makes SERS a promising low-cost and real-time tool for biomedical applications [29–36].

Unfortunately, SERS of biomolecules still suffers a lack of reproducibility due to arbitrary chemical sorption and superficial interactions between the analyte and the metal, possible toxicity of metallic nanoparticles, masking SERS signals by surfactants or by-products [35–45]. Commonly used linkers, surfactants, reducing agents and their oxidized forms, halide ions etc. can affect both nanoparticles and biomolecules, prevent a target molecule to approach a close proximity of nanoparticles or change characteristic properties of nanoparticles because of their aging, recrystallization or random formation of aggregates. Nanostructured substrates promise better reproducibility and less toxicity promoting their SERS applications in biology and medicine like rapid monitoring of living cells and their organelles [35, 37, 39, 45]. Superficial roughness of the substrates can be created by deposition of metal colloids onto surfaces, coupling between continuous metal films and plasmonic particles, vapor deposition of metals, nanocasting and lithography, electrochemical deposition through a template of self-assembled latex spheres, abridging pillar tip spacing by sputtering, self-assembly of large-scale and ultrathin nanoplate films, application of porous substrates [31–33]. This makes the developing field of SERS studies highly stimulating for future single-molecule, single-cell or single-organelle diagnostics as discussed in this short review.

Redox chemistry of the diamminesilver complex

The most known and prominent silver precursor is diamminesilver (I) hydroxide or the Tollence's reagent. Actually, this is not only a typical oxidizer in a pair with reduction substances, it may alone produce pure silver nanoparticles without any byproduct [42–45]. This comes (Fig. 2) from drastic stabilization of silver (I) ions within the complex ($K_{stab}([Ag(NH_3)_2]^+) = 1.3*10^7$, $Ag^+ + 2NH_3 = [Ag(NH_3)_2]^+$), combined with a large redox potential of silver ($E^0_{Ag/Ag+} = 0.8$ V) in the absence of ammonia, a possibility to precipitate the Ag_2O solid phase or dissolve it by ammonia ($Ag_2O + H_2O + 4NH_3 = 2[Ag(NH_3)_2]^+ + 2OH^-$) and, finally, the absence of other anions in the redox system, except OH^-, which is a natural part of all the aqueous solutions ($Kw = [H^+][OH^-] = 10^{-14}$). Another part of the system is oxygen which can be dissolved in the solution as an oxidizing agent or evolved from the solution as a product of silver oxide decay, since the standard potential of the pair O_2/OH^- E^0O_2/OH^- is equal to 0.401 V.

The overall reaction $Ag + ¼\ O_2 + 2NH_3 + ½H_2O = [Ag(NH_3)_2]^+ + OH^-$ (1) serves as a good control tool for generation of silver nanoparticles simply by changing of the concentration of ammonia to generate enough Ag + ions reducing into metallic silver, otherwise Ag^+ is stabilized as $[Ag(NH_3)_2]^+$ and can not be reduced under given conditions. The electrode potentials for the redox pairs are the follows:

$$O_2 + 2H_2O + 4e = 4OH^-,\ E_{O_2/OH^-} = 0.401 + 1/4*0.059 + 1g\left(P_{O_2}/[OH^-]^4\right),$$

$$Ag = Ag^+ + e,\ E_{Ag/Ag^+} = 0.8 + 0.059 * 1g[Ag^+].$$

The overall redox potential is a combination of the above reaction potentials, $EO_2/OH^- - EAg/Ag^+$, or, for $PO_2 = 0.21$ atm, $E = (-0.399-0.01*\gamma)-0.059*\gamma*1g([OH^-][Ag^+])$ where $\gamma = T/298$ gives the potential change with temperature. "Free" $[Ag^+]$ is expressed by the ratio $[Ag(NH_3)_2^+]/(K_{stab}*[NH_3]^2)$ while electroneutrality conditions dictate that $[OH^-] = [Ag(NH_3)_2^+] + [Ag^+] + (1.8*10^{-5}*[NH_3])^{1/2}$. The latter comes from OH^- generation in ammonia solutions, $NH_3 + H_2O = NH_4^+ + OH^-$ ($K_{amm} = 1.8*10^{-5}$) although $[Ag(NH_3)_2^+]$ dominates since NH_3 is a weak base and contributes negligibly. The calculated data are presented in Fig. 2. It is evident that even small concentrations of ammonia makes the reaction to shift to the right side forming $[Ag(NH_3)_2]^+$, no silver nanoparticles could be formed. However, if the NH_3 ligand is lost by evolving from the solution, there is an area of negative potentials where diamminesilver (I) hydroxide is not stable thermodynamically and decomposes forming metallic silver nanoparticles. The ABC pathway means a starting point of a high concentration of separately prepared $[Ag(NH_3)_2]^+$ in an excess of ammonia then a sharp drop of the concentration of ammonia should happen, for example, due to the ligand evaporation with partial decomposition of the complex, and then the process ends up at a very small concentration of $[Ag(NH_3)_2]^+$ and a higher concentration of "naked" silver ions transforming into isotropic silver nanoparticles [44].

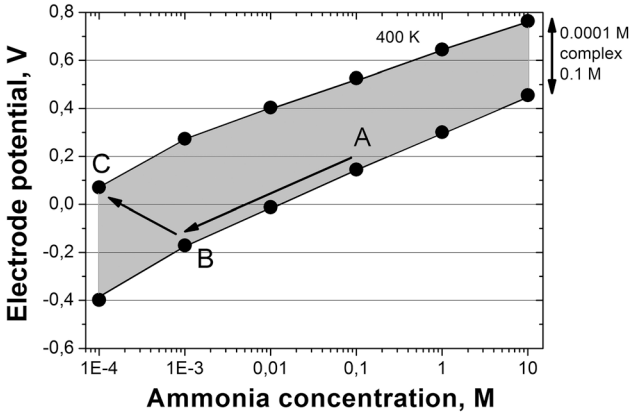

Fig. 2: Calculated electrochemical potentials of the reaction $Ag + 1/4O_2 + 2NH_3 + 1/2H_2O = [Ag(NH_3)_2]^+ + OH^-$ as a function of ammonia concentration in boiling water, the lower curve is equal to 0.1 M concentrations of $[Ag(NH_3)_2^+]$, the upper one is the diluted 10^{-4}M solution of the complex. The ABC path corresponds to the formation of silver [42–45].

Random faceting, skeleton and mesocage particles

Anisotropic silver nanoparticles or nanoparticles with complex shapes possess better perspectives of practical applications as compared to silver nanospheres. In particular, pseudomorphs (mesocages) of metallic silver appear upon a shape-preserving reduction of polyhedral precursors of silver (I) oxide either with hydrogen peroxide in aqueous ammonia (Fig. 3) or after ultrasonic spray pyrolysis of aqueous diamminesilver (I) hydroxide (Fig. 4). They are revealed as promising SERS-active materials with morphologically predetermined hot spots, a wide light absorption range spreading over the narrow plasmonic bands of separated AgNPs and, also, an enhanced surface area available for sensing of target adsorbed substances [43, 49, 50].

An overall morphology of the polyhedra prepared by the PVP (polyvinylpyrrolidone) protocol [49, 50] demonstrates that the octahedral particles are the centers of silver regrowth and the secondary nucleation sites as proved by the observation of additional silver seeds deposited onto facets of some octahedra. Each of the particles consists of 20–40 nm silver clusters forming pseudomorphic octahedral shapes with a large number of pores increasing partly the overall surface area and, what is even more important, providing capillary channels for analytes to reach the "hot spots" in the pseudomorphs (Fig. 3). Thus the pseudomorphs consist of pure metallic silver with disordered polycrystalline structure; the same is confirmed by the presence of multiple nanosized pores and quite rough surface of the octahedra.

Pure silver nanoparticles with a complex morphology prepared directly using ultrasonic aerosol spray pyrolysis (ASP) of aqueous diamminesilver (I) hydroxide include porous spheroids, cuboids and more complex overgrowth structures (Fig. 4). The growth features seem to be connected with fast decomposition of diamminesilver (I) hydroxide in mist droplets and its reduction to pure silver therefore this precursor, as compared to other salts and complexes, gives a large benefit owing to simplicity, promptness and low temperature conditions of the production process, typically about 250 °C, to obtain new types of nanoparticle morphologies suitable for SERS.

The ASP process is complex due to peculiarities of chemical transformation of silver complexes. The thermal treatment of ultrasonic mist within a hot zone provides irreversible decomposition of the major part of the initial silver complex and also quick solvent evaporation. The products of this transformation include silver nanostructured particles, water, ammonia and oxygen, also molecular oxygen contacting the products from surrounding air. Quenching such reaction products gives nanostructured particles and their aggregates formed in a shock manner, since the whole transformation occurs quickly, for seconds, and at the highest temperatures used. Oppositely, nanostructured silver particles have a chance to undergo further prolonged transformations in the condensation zone because the temperature is high enough to promote redox processes in water solution containing the suspended particles, residual traces of the silver complex and ammonia dissolved back from a vapor phase.

The polyhedral aggregates would be a consequence of primary silver (I) oxide formation within the mist droplets prior its transformation into nanostrustructured silver. Ag_2O is able to produce cubic, edge- and

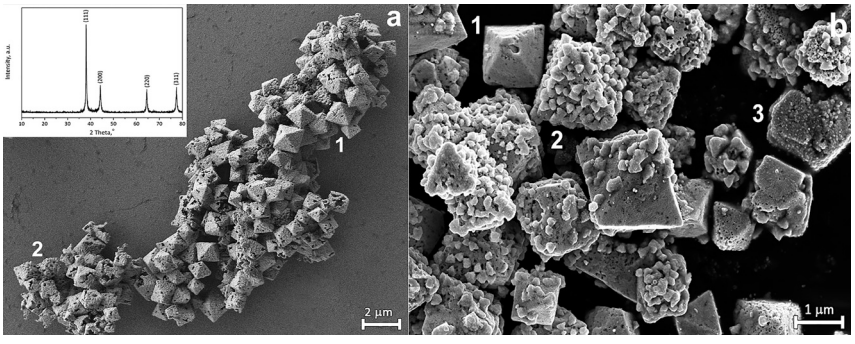

Fig. 3: Metallic silver nanostructured particles obtained by pseudomorphic reduction of octahedral Ag_2O with hydrogen peroxide in aqueous ammonia. (a) a general and (b) magnified views of the precipitate (the inset shows an XRD pattern of cubic silver), 1 – smooth morphology, 2 – octahedra overgrown with AgNPs, 3 – intergrown pseudomorphic silver.

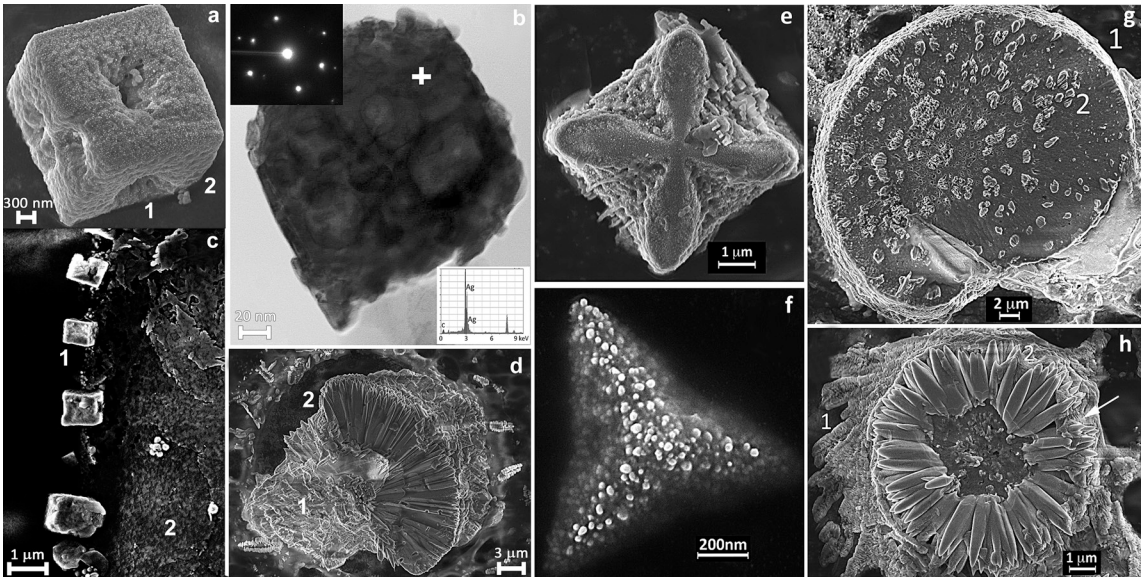

Fig. 4: Complex morphology of nanostructured particles from a condensation zone found after ultrasonic spray pyrolysis of aqueous diamminesilver (I) hydroxide. (a) cross – centered cuboids and their TEM/ED investigation (b), (c) a necklace morphology of silver nanostructured particles, (d) a nanoflower, (e) overgrowth of facetted cuboid, (f) triangles, (g, h) stem – flower structures.

corner-truncated cubic, rhombicuboctahedral, edge- and corner-truncated octahedral, octahedral, and hexapod structures and they could then transform into pure silver forming pores due to oxygen liberation and the mismatch of lattice parameters of silver (I) oxide and metallic silver. In particular, the formation mechanism of cross – centered cuboids and starfish nanostructured particles [43] resembles growth of skeleton forms of crystals under highly nonequilibrium conditions with a lack of nutrient phase; thus flat facet growth is replaced with development of quickly growing rough grains and dendrites. Growth of "porous bundles" and nanoflowers (Fig. 4) seems to be the different stages of the same process of Ag_2O thermochemical transformation followed by kinetically controlled development of the fastest growing co-oriented grains reproducing the initial texture of the bundles. This is confirmed by the feature of penetration of growing "flower petal" through the "stem" and the tubular-like assemblage of the bundle. The cuboids (Fig. 4) seem not to be single crystalline. Their size enlargement occurs due to post-reduction of silver in the presence of remaining byproducts and overgrowth of the initial particles. The metallic silver cuboids could be thus considered as pseudocrystals formed in a topotactic manner preserving the shape of precursor crystals of silver (I) oxide usually crystallized as cubes [49]. An additional feature observed for most of complex morphologies is the heterogeneously formed nanoparticles decorating the surfaces of larger particles. They are shapeless and sized within the range of 10–50 nm. The mechanism of their formation is related to the peculiarities of interaction of silver nanostructures and the liquid solution [49]. The size of building blocks of the silver structures obtained by both the PVP and ASP protocols are favorable for implementation of them into SERS devices [43, 49, 50].

Controlled faceting and anisotropic particle shapes

One of the most promising families of nanostructured silver materials comprises prisms, triangles, discs and other platelet-like anisotropic silver nanoparticles [32, 36, 51–58]. In particular, they are highly desired for future applications of SERS since biological objects demonstrate a wide diversity of optical properties, consequently, anisotropic silver nanoparticles can be adjusted to the exact biological sample due to their highly tunable plasmon resonance features (Figs. 5 and 6). Anisotropic silver nanoparticles in aqueous media (Fig. 5) are formed usually from primary silver seeds followed by selective grain growth in the presence of PVP

and/or citrate ions [32, 52–58]. PVP stabilizes silver seeds with diameters less than a certain critical size required for morphological transformation, while citrate is critical to induce the nanoplate formation, by preferential binding onto (111) planes. AgNPs formed in the absence of halides and PVP, show truncated triangular and hexagonal morphologies, whereas an addition of bromides leads to rounding of the edges and then to compaction into dominant cubic and bipyramidal geometries. Rounding occurs due to etching of the most highly energetic protruding edges. Observation of twinned cubic and bipyramidal particles is consistent with the structural transformation since bromide exhibits a strong tendency to stabilize (100) facets in AgNPs and to induce the formation of corresponding 3D shapes. Chlorides bind more weakly to silver ions and to the surface of growing AgNPs as compared to bromide therefore significantly higher chloride concentrations are required to affect AgNP formation. However microscopic, optical and particle size distribution measurements reveal re-crystallization of the primary silver nanoparticles to larger crystallites after the NaCl addition (Fig. 5).

Silver nanoplatelets form highly stable colored sols effectively absorbing light even at very diluted concentrations (Fig. 5). Absorption spectra and positions of plasmonic bands with dipole and quadrupole resonances evidence for the formation of anisotropic nanoparticles although intensity of exact plasmonic peaks are smoothed and the positions are gradually shifted compared to theoretical predictions (Figs. 5 and 6). The

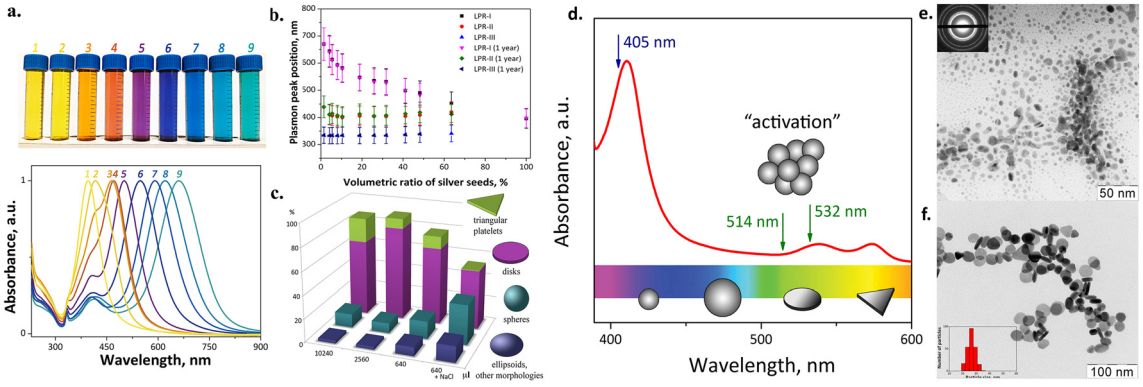

Fig. 5: General view and normalized UV-vis spectra (a) of silver sols with anisotropic silver nanoparticles obtained using nanoparticle secondary growth with different amounts of the seeding solution, (b). positions of plasmonic bands with dipole (I) and quadrupole (II, III) resonances for silver sols before and after 1 year of aging, (c). particle fractions for some samples of silver nanoplatelets, in the (a) graph of the samples with a different amount of the seeded solution (in microliters) as compared to 1% NaCl solution admixing (the "+NaCl" notation), adopted from [51], (d) a conceptual scheme of light absorption maxima of different types of silver nanoparticles compared to the Soret and beta-bands of erythrocytes, (e) TEM of spherical and (f) disk and triangular-like silver nanoparticles.

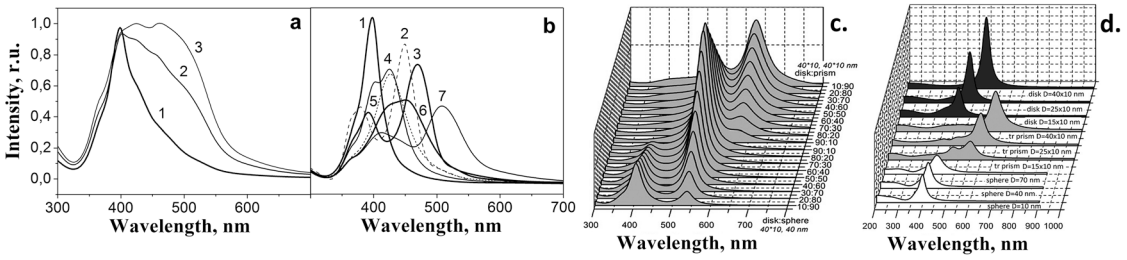

Fig. 6: Optical properties of silver sols. (a) simulated extinction spectra of nanoparticle ensembles for mixtures of 70*70*105, 40*40*60, 70*70*84, 40*40*48 nm ellipsoids and 10 nm spheres with their contributions (%) of 10:10:10:30:50 (1), 35:10:35:10:10 (2) and 50:20:20:10:0 (3), respectively; (b) spectral components of the simulated spectra, 10 nm (1) and 70 nm (5) spheres, 10*10*15 nm (2), 40*40*60 nm (3), 40*40*48 nm (4), 70*70*84 (6), 70*70*105 nm (7) ellipsoids, respectively, (c) Discrete Dipole Approximation (DDA) of extinction spectra of nanoparticle ensembles (mixtures of fractions, the contributions are given in the picture). (d) DDA simulation of extinction spectra of nanoparticle ensembles (single fractions) with different morphologies of silver nanoparticles, spheres, discs and triangular prisms of different sizes.

reason originates from mixing of different fractions of silver nanoparticles as dependent strongly on preparations conditions and, in the most valuable extent, on the amount of silver seed added at the first stage of the nanoplatelets growth [51]. However in all the cases, except silver seeds themselves, several types of nanoparticles can be found including rounded ellipsoids, prisms, discs, triangular an hexagonal plates (Fig. 5). Each fraction gives an additive contribution to the light absorption spectra and, correspondingly, to the color of the sols, that is why the experimental data are a superposition of several subspectra with the main peaks attributed to a dominating fraction.

Anisotropic silver nanoparticles are needed to cover all demanded light absorption ranges since their anisotropy predetermines the plasmonic peak positions (Fig. 5). To clarify the statement of additivity as a property of the absorption spectra of silver nanoplatelet ensembles, the discrete dipole approximation (DDA) method was used to simulate optical properties of the silver sols for aqeous surrounding [39]. It is assumed that each nanoparticle makes its own contribution to the extinction spectrum independently on the neighbor particles in diluted sols. As evident from Fig. 6, an ensemble of spherical particles can not physically give a broad extinction spectrum observed experimentally since isotropic particles have a narrow plasmon peak and, moreover, this peak shifts by 15–20 nm only to the red side even if the particle size becomes several times larger. If anisotropic silver nanoparticles are present, while a fraction of the smallest isotropic 10 nm nanoparticles is negligible, the spectrum is broadened, absorption occurs at the blue and red shoulders of the spectrum. Actually, there is always a possibility that a median of the spectra corresponds to nothing real in terms of an exact size and shape of the nanoparticles since this is a sum curve of different contributions from several fractions of the nanoparticle ensemble.

At the same time, a nanoparticle mixture is favorable for an advanced design of universal substrates for the SERS analysis. It is known that SERS amplification demands a close proximity contact of the object and the nanostructures since the SERS effect vanishes quickly at distances more than 15–20 nm; the resonant effects play a great role in this analysis. Therefore it does not really matter how broad the nanoparticle distribution is, since only a proper fraction of nanoparticles, matching both the absorption range of the analyte molecule and the laser excitation wavelength, predominates. This assumption leads to a set of ideas concerning the SERS analysis: a mixture of anisotropic silver nanoparticles could be used universally to achieve a broad integral absorption with uniform contributions of many fractions of nanoparticles suitable for a given analyte and also widespread excitation lasers; the nanoparticles are better immobilized on a scaffold to increase a contact area with living cells or organelles and to reduce the ability of nanoparticles to aggregate as it leads usually to unpredictable changes of their optical properties; nanoparticle surrounding should not affect their size and, more importantly, their shape thus keeping the benefit of anisotropic nanoplatelets in terms of advanced plasmonic modes and SERS effectiveness [39, 51].

A key issue of practical applications of silver nanomaterials is related to their aging and stability. At the same time, proper preparation conditions lead to stable silver nanoplatelets having no tendency to increase their size or change their shape spontaneously (Fig. 5). Silver sols stabilized with PVP preserve their optical properties; main absorption modes are shifted slightly only after 1–5 years of storage (Fig. 5). It is also obvious (Fig. 5) that an addition of pure NaCl in the concentrations comparable to that of the physiological saline to the colored sols containing anisotropic silver nanoparticles causes irreversible, catastrophic changes of their optical properties in a couple of minutes, in particular, leading to a pronounced blue shift by about 100–150 nm and narrowing the peaks [51]. The main reason of these changes is connected with that discs and elongated rounded nanoparticles (ellipse-like) transform into the most isotropic, spherical nanoparticles after the addition of chloride ions.

Therefore anisotropic nanoparticles are not compatible with commonly used halide-contained saline needed to preserve biological objects in their intact form [34, 39, 51]. Silver has only a few soluble salts and the only salt with an anion of a strong acid is known to be silver nitrate, $AgNO_3$. Therefore to prevent the observed recrystallization of silver platelets, which takes place under the action of chloride ions, we should choose another cell incubation medium based on the physiological buffer solutions in which chloride ions are replaced by NO_3^-. Silver nanoplatelets do not have a tendency to increase their size or change their shape spontaneously if surfactants and nitrate ions are present in the colloidal solution (Fig. 5). The replacement of

chloride ions with nitrates has no dramatic effect on the cell integrity or shapes and therefore this solution is suitable to provide SERS tests with native erythrocytes and other biological objects [51].

Silver nanofibers of about 100 nm in diameter and 30–50 μm long (Fig. 7) are prepared using the polyol method [59, 60]. The electron diffraction pattern (Fig. 7) evidences that the fibers are metallic silver. Formation and growth of silver nanowires are caused by the deposition of silver add-atoms on the {111} planes of silver particles. These facets are atomically rough compared to the flat {100} grains that is why supersaturation relaxes in the course of polyol process by fast deposition of add-atoms onto these particular grains providing highly anisotropic growth of the fibers. Additionally, a stronger surface interaction of PVP with {100} planes can lead kinetically to the growth of 1D nanostructure.

Generally, for the FCC metals like silver, the {111} facets are the most stable facets among the three (111, 110 and 100) ones, the {100} facets are the next stable, and the {110} are the least stable. The growth rate of {110} facets should be fast in the absence of surfactants or polymers affecting the resultant aspect ratio of the nanowires. The free energy minimization could result in preferential growth if PVP is strongly attached to the {100} facets. The twinned silver nanowires could thus arise from a selective interaction between the PVP molecules and the {100} planes [59]. Usually observed penta-twinned crystal with a 5-fold axis, which was shared by two {111} facets, could be formed by stacking faults because the angular mismatch should result in a lattice distortion in the silver nanowires, and the atoms surrounding the radial direction had to offset the mismatch by crystal strain and dislocations. The crystal strain would increase for larger diameters of nanowires thus restricting the lateral growth of silver nanowires and giving 1D structures. This would result to the observed extended defects like 45°-angled screw dislocations within a 5–20 nm distance between each other and spreading from a middle to the surface of the nanofibers (Fig. 7) since the observed dislocations should be associated with stacking faults or twinning.

Silver ring stochastic substrates

SERS conquests quickly the niche of ecological and biomedical diagnostics [4, 9, 29, 36, 39] however these efforts still demand the development of new SERS active materials. Recently, nanostructured silver coatings with an hierarchic “coffee ring” morphology for SERS of various families of analytes are produced by superficial decomposition of ultrasonic mist of aqueous diamminesilver (I) hydroxide free of reducing agents and

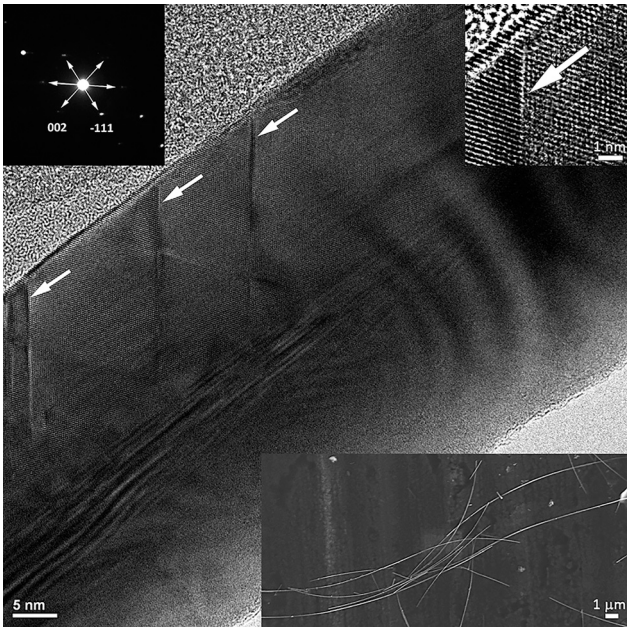

Fig. 7: HREM micrograph of silver nanofibers morphology obtained using the 0.25 M $AgNO_3$ solution and 160 °C preparation temperature. The arrows indicate extended effects. An SEM view of the nanofibers at a low magnification is shown as a bottom inset. The upper left inset corresponds to a ED pattern and the upper right inset shows a magnified view of an extended defect.

non-volatile pollutants [35, 36, 39, 45]. In the case of application of warm substrates, silver ring structures are formed at moderate temperatures of 200–250 °C due to deposition of the mist droplets onto a preheated substrate (Fig. 8). The coatings consist of overlapping rings of a complex morphology originated from decomposition of micron-sized droplets of ultrasonic mist. This resembles a rain making rings on a dusty surface therefore we call it UltraSonic Silver Rain. Usually, silver deposition gives intersecting circles of 30–100 μm in diameter. This value is several times larger than the expected size of 1–10 μm of the falling mist droplets because the liquid from the droplets spreads laterally over the substrate. Solvent evaporation increases concentration of the silver complex and then metallic silver resides on rims of the spreading circles producing walls of silver rings.

The thickness of walls is found to be typically within 1–3 μm while the residual part in between is covered with randomly distributed silver nanoclusters gradually increasing sizes from 10–20 nm in the centers of the circles to about 100 nm in the wall vicinities. The nanoclusters increase the role of capillary forces and then more droplets stack onto the surface and boil; an increase of sputtering time leads to rough and porous layers (Fig. 8). This deposition mode has several advantages in terms of formation of SERS-active structures for promising applications: silver micro- and nanostructures are immobilized onto a substrate and form a rather stable metallic film on cheap materials like glass, there is no need to filter or separate nanoparticles, the nanostructure consists of porous silver sponge, the temperatures are high enough for the one-stage formation of pure metallic silver nanostructured layer with no remaining byproducts; this preparation route is effortless and can be reproduced easily in common laboratory practice [35, 36, 39, 45].

The complicated circular morphology of the nanostructured silver coatings might be caused by the known "coffee ring" effect [35, 36, 39, 45] involving a wide variety of processes including contact-line motion, directed assembly, thermal and solutal Marangoni flow, flow instabilities, and the formation of a surface-skin. Indeed, if a drop of liquid dries on a solid surface forming nanoparticles, the latter would be deposited in a ring-like fashion. During the drying process, drop edges become pinned to the substrate, and capillary flow outward from the center of the drop brings suspended particles to the edge as evaporation proceeds. The particles are

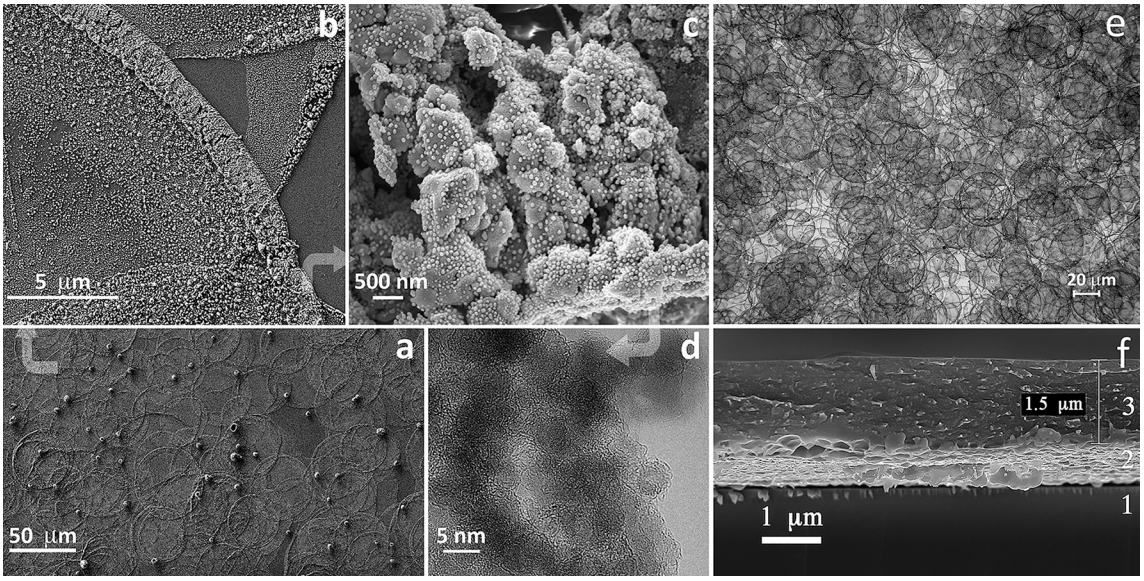

Fig. 8: Hierarchical structure of "coffee ring" coatings (AgNSS). (a) general view, SEM image of intersecting silver rings with spherical nanostructure aggregates; (b) silver ring wall contouring an evaporated droplet of the silver (I) complex, magnified SEM view, a gradually increased population of silver clusters inside the ring is observed; (c) silver sponge of the ring rims, another magnification of the SEM graph, the rim of the rings consists of blocks superficially covered with 20–40 nm silver nanoparticles; (d) high resolution TEM image of the silver sponge consisting of 2–10 nm silver nanoparticles with a number of "hot point" contacts and empty channels between the smallest AgNPs serving as building units for the whole structure; (e) overall low-resolution optical image of the substrate surface; (f) the substrate cross-section.

left highly concentrated along the original drop edge. As soon as the formed nanoparticles are moved to the rim by the outward flow, their local attractions lead to the formation of loosely packed structures near the rim. These structures prevent the suspended particles from reaching the droplet edge and make deposition more uniform. The complexity of the "coffee ring" scenario yields the observed unusual structures for all the silver-ring substrates.

The silver ring formation process is accompanied by nanostructuring onto the substrates. When silver forms, large and smaller gaps appear in the region of rims and this gives random blocks ("bricks" of the wall) of 200–500 nm (Fig. 8). The bricks and the walls are composed of nanometer-sized interconnected silver particles because an every act of droplet transformation on the substrate gives newborn AgNPs of a very small size of several nanometers. Latter, these nanoparticles grow, join each other and form channels resulting in the observed high porosity of the silver walls. Instant capillary transport of nutrient solution to the top of walls through the channels leads to growth of 20–40 nm grains of silver covering the bricks. A thorough inspection allows to assume that dissolution of neighbor smaller nanoparticles of the matrix supplies further growth of larger "sesame seeds". All the elements of this hierarchical structure are conducting and that gives a variety of possibilities for plasmon coupling.

A number of plasmonic bands appear for these nanostructured substrates with pure silver thus forming a very wide light absorption band with a long tail towards larger wavelengths because of the hierarchic nature of the coatings described above; this allows to use the most popular lasers with 514, 532, 633 and 785 wavelengths to agitate plasmons and plasmon-polaritons while much narrower peaks observed, for example, for separated nanoparticles and sols make them less effective in terms of enhancement of Raman signals for particular lasers. The substrates demonstrate excellent plasmonic behavior exceeding the same parameter for AgNPs sols immediately after their fast and easy preparation without applying an additional treatment [36, 39, 45]. Thermal decomposition of diamminesilver (I) hydroxide solutions allows the preparation of nanostructured silver materials with an uniformly low background signal and the latter becomes possible because of a combination of highly nonequilibrium preparation conditions guaranteeing a small size of forming nanoparticles and their aggregates and also a high enough temperatures preventing physical adsorption and chemisorption of byproducts. Moreover, aerosol deposition is a scalable method suitable for preparation of either nanoparticles of a complex shape or planar nanostructures with a large number of "hot spots".

Such a hierarchic structure with a multilevel arrangement of AgNPs can result in a significant increase of electric fields near AgNPs, in better immobilization of biological objects on AgNSS, and in the higher number of contact sites of the objects with AgNSS. A reasonable explanation of the observed surface-enhanced Raman scattering is based on several known facts related to the problem of light scattering by metal nanoparticles located near a metal surface. If the size of nanoparticles is much smaller than the wavelength of incident light, the nanoparticle can be considered as an electric dipolar scatterer with a corresponding dipolar polarizability, and the induced dipole moment of this nanoparticle is determined by the incident and reflected electric fields and by nanoparticle-surface interaction. Following this, the dipole moment vectors of the real electric dipole and its image have opposite (or the same) directions, when the real electric dipole aligned parallel (or perpendicular) to the surface [35]. Due to such dipole-surface interaction, the in-plane components of the dipole moment are decreased and the normal component is increased. Thus, if the induced electric dipole moment of the nanoparticle located on metal surface has mainly the normal component, a strong electric near field enhancement can be produced. The multiscale inhomogeneous distribution of nanoparticles onto the AgNSSs enables excitation of strong electric near-fields in the system [35]. Since many nanoparticles of the AgNSS ring substrates are located on side walls of different cavities, they are irradiated by polarized light under the incline conditions with respect to the surface. As the result, the light electric field directed perpendicular to the side walls of the cavities will induce strong nanoparticle's electric dipole moments. This will lead to the induction of strong nanoparticle's electric dipole moments by the light electric field directed perpendicular to the side walls of the cavities. The distribution of these electric fields can be imagined as electric-field "needles" deeply penetrating into the biological objects. In this case, the contact area between the biological cells or their compartments and the nanoparticle structure is also increased providing better conditions for SERS [35].

Colloidosomes and nanocomposites

Silver nanocomposite materials attract permanent interest in various applications due to their unique properties as catalysts or building blocks of complex materials with strong plasmon resonance for advanced SERS applications in biology, medicine and ecology. An effective strategy to design SERS-active materials is based on preparation of nanocomposites composed of microparticles like Stoeber-derived silica microbeads [61] decorated with nanoparticles [36, 39, 41, 42, 62–64]. Such materials allow to concentrate nanoparticles on the surface of dielectric microcarriers, to organize additional hot spots, to build up self-assembling structures and to control optical properties by thickness and coverage of the SiO_2 core by the silver shell.

Usually, silver reduction agents like ascorbic acid, $NaBH_4$, Sn(II), polyvinylpyrrolidone (PVP) are used to produce and electrostatically attract silver nanoparticles to the surface of silica [62–64] while it is shown in a number of recent papers that diamminesilver (I) hydroxide complexes can be used alone to produce silver nanoparticles under mild conditions [36, 39, 41, 42]. Traditional generation strategies of heterogeneously seeded SiO_2 microspheres include either separate preparation of silver seeds by homogeneous nucleation followed by their electrostatic attachment to silica or forming special superficial groups or chemisorbed reducing agents to provide predominant formation of silver seeds directly onto the surface of silica. We consider another, much simpler and effective, way supported by our previous works which is based on gradual self-reduction of one of the most useful and well-known ammonia complex of silver, $[Ag(NH_3)_2]^+$, due the lost of its stability upon the ammonia ligand leakage, as described above [36, 39, 41, 42].

The experimental ABC reaction pathway (Fig. 2) is accomplished after boiling the silver complex together with silica beads. The silver-silica nanocomposite forms after the interaction of hot silver complex with silica beads as seen from TEM images, SAED and XRD data (Fig. 9). A typical size of the isotropic silver nanoparticles embedded (encrusted) into the superficial layer of silica is surprisingly small, only about 2–5 nm, and demonstrates no large deviation in the mean size. The observed seeding nanoparticles are spherical while longer time or repeated treatment with a hot silver complex could cause formation of new, larger, overgrown nanoparticles of silver of about 20–25 nm in diameter and those particles are twinned or polycrystalline. In all the above given cases, no polygonal, polyhedral or distinctly facetted particles are found. Another feature of the silica beads treated in a hot solution of the diamminesilver (I) hydroxide complex is superficial etching (Fig. 9). It seems that this etching process is important for further overgrowth of silver since many originally formed seeding nanoparticles go deeply into the body of silica microspheres, they are encrusted into the superficial layer but not simply attach to the surface, as typical for traditional methods (Fig. 10).

In order to modify optical properties of the nanocomposites, it is necessary to transform the seeds on the surface of silica into anisotropic nanoparticles. This becomes possible if a second, overgrowth, stage is used

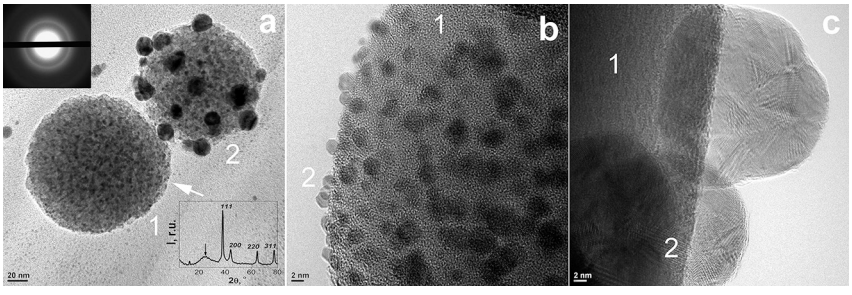

Fig. 9: Typical TEM images of silica beads after treating with a hot solution of $Ag[(NH_3)_2]OH$. (a) Two fractions of silver-silica nanocomposites, 1 – major fraction of Stoeber silica microspheres with incorporated 2–5 nm silver seeds (1), and a minor fraction with both seeds and as grown 15–20 nm silver nanoparticles (2), the arrow indicates silica surface etched by the base solution of $Ag[(NH_3)_2]OH$ with increased OH^- concentration compared to aqueous NH_3. The upper inset shows SAED data for the major fraction, the lower inset gives the overall XRD pattern of the dried sample, the arrow shows the presence of amorphous silica, (b) the beads with seeds and (c) magnified micrograph with silica microspheres and silver nanoparticles, 1 – silica microsphere matrix, 2 – silver seeds or nanoparticles.

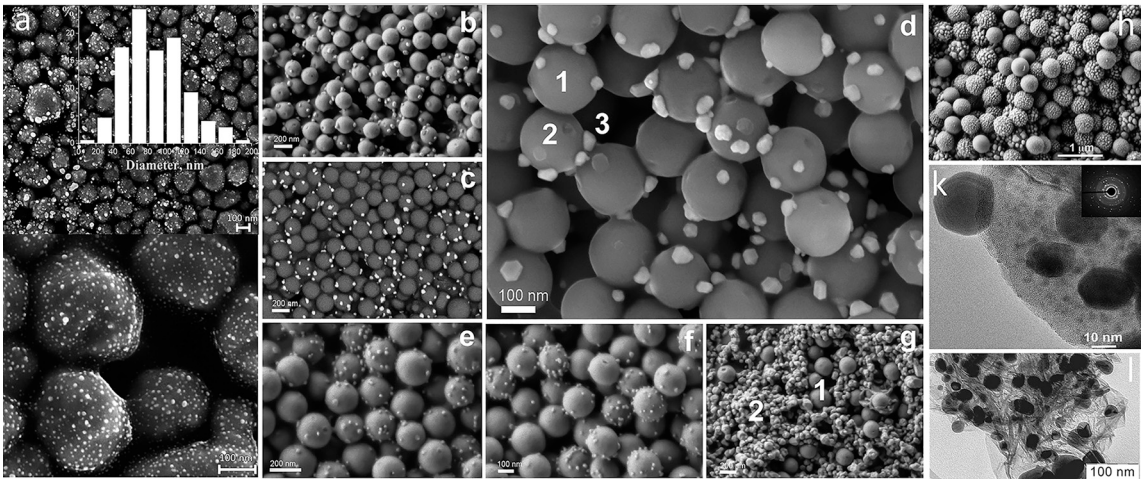

Fig. 10: Microstructural features of silver-silica composites (colloidosomes). (a) SEM view of pollen-like self-composite of silver, (b–g) SEM micrographs of the samples prepared with various concentrations of ascorbic acid and silver nitrate, (d) magnified SEM view of the sample with anisometric silver nanoparticles showing silica beads (1), pits (2) on the surface of silica and polygonal silver nanoparticles (3), (h, k) SEM and TEM images of the colloidosomes prepared using the ASP techniques and the diamminesilver (I) hydroxide precursor, (l) TEM image of the graphen oxide (GO) – Ag colloidosomes prepared using the same ASP technique.

(Fig. 10b and d). The ascorbic acid is a strong reducing agent with respect to silver ions and thus mixing of silver nitrate solutions with even diluted solutions of ascorbic acid leads to immediate deposition of black metallic silver (Fig. 10g). This occurs due to homogeneous nucleation of silver after a redox reaction and fast growth of silver particles above 100 nm. The latter is not plausible since silver is formed everywhere in the bulk solution while coverage of silica by silver remains insufficient; such a large particle size gives, as well-known, materials with small SERS effectiveness. A decrease in the concentration of the solutions for overgrowth prevents homogeneous nucleation but remains effective for seeded growth of silver nanoparticles directly attached onto the surface of silica beads [41, 42]. As a result, homogeneous nucleation barrier is not overcome and only heterogeneous nucleation proceeds. The most intriguing feature of such samples is the formation of unusual facetted / polyhedral silver nanoparticles on the surface of silica beads (Fig. 10d). Therefore overgrowth in diluted solutions of silver nitrate and ascorbic acid provides predominantly heterogeneous nucleation followed by anisotropic particle formation without application of usual surfactants or citrate ions known to produces such nanoparticles due to selective grain growth. The particles (Fig. 10d) are not electrostatically attached to the surface, as usual, but encrusted due to overgrowth from the seeding particles resided in small concaved pits formed by the surface etching with alkaline ammonia complex of silver during the seeding stage. It should be noted that the shape of many particles is not cubic as typical of the equilibrium habitus of FCC phases. The triangles, angled triangles grow on the surface of silica; the observed hexagonal platelets present a quite unusual shape of facetted silver nanoparticles keeping in mind free growth of the nanoparticles without usual surfactants like PVP or citrate ions.

Such a nanocomposite reveals evidently a pronounced red shift of the plasmonic band [41, 42], actually till the beginning of the common light absorption range of spherical gold nanoparticles (~520 nm). This is observed visually as an unusual deep purple color of thin concentrated layers of the nanocomposite within a xerogel of ethylcellulose, the dichroism typical of anisotropic nanopaticle ensembles is also found as a greenish color under reflection conditions [42]. Most probably that the observed hexagonal nanoplates have an FCC structure and the (111) planes are the basal planes of the nanoplates. The two lateral faces are consistent with (100) and (111) faces. It is possible that the nanoplates appear as flat crystals with two (111) faces at the top and the bottom, limited by three straight (111) faces at the edges and by three (100) faces at the corners, thus the shape becomes hexagonal.

The pollen-like silver nanoparticles (PLiS, self-composite, Fig. 10a) were prepared by a two-step procedure including the formation of original silver nanoparticles and their *chimie douce* superficial self-decoration [60]. The transformation takes 5–7 days and is characterized by both a 1–2 day incubation period for dissolving the particles across extended defects and smoothing the edges of polyhedral globules followed by silver re-deposition in a form of superficial roughening of the nanoparticles. The major steps of the whole process are caused by step-by-step etching of metallic silver with gaseous oxygen dissolved in aqueous ammonia due to silver (I) stabilization within a soluble ammonia complex, the complex accumulation as an intermediate product and its consecutive gradual decay into nanosilver because of the ligand loss and the above described redox reaction of silver (I) and NH_3. The as-formed metallic silver deposits onto larger silver particles heterogeneously decorating their surface; this broadens the initial plasmonic peak and causes a weak red shift because of nanostructuring and particle size distribution features. The latter makes a substantial contribution to the overall optical properties of the nanoparticles of a complex morphology and has to be considered as an important factor affecting optical characteristics of nanoparticle ensembles.

Elevating the temperature allows to utilize the aerosol spray pyrolysis techniques for production of nanocomposites with various matrixes (Fig. 10h–l). ASP is known as an effective streaming and scalable method based on spraying of micron-sized droplets of precursor solutions and their fast nonequilibrium transformation under high temperatures into solid phases and nanostructured materials [35–37, 39, 41, 43, 45]; the droplets play the role of microreactors providing often such the nanostructuring. In particular, the carrier material could be represented by solid inorganic micro- or nanoparticles like graphene oxide (GO) flakes, magnetic superparamagnetic iron oxide nanoparticles (SPIONs), or dielectric biocompatible silica microspheres [65]. In the first two cases, it is expected that the nanoparticles can be self-assembled into hollow microspheres composed of the mixture of silver nanoparticles and the original inorganic nanoparticles present in the suspension. Iron (II) ions of Fe_3O_4 or functional groups of GO would cause initial silver ion reduction (Fig. 10l). In general, this method is universal and would give various materials (dielectric, magnetic, samples with an increased specific surface area) combined with SERS-active silver nanoparticles in one step.

The reaction of silver formation takes place in aerosol droplets and the final powder does not accompanied by side products and thus it requires no purification, it takes also short preparation time. Thus the spraying process in the case of silica (Fig. 10h) allows to produce SERS-active silica beads coated with silver nanoparticles and a smooth Raman background suitable for measurements of biological objects [41]. Different sizes of silver superficial aggregates originate of different volumes of aerosol droplets providing increased or decreased amounts of dissolved silver for each SiO_2 microsphere entrapped by a droplet of aqueous silver complex in streaming aerosol. Due to a high enough concentration of silica colloid used for spraying, almost all the silver nanoparticles reside onto the surface of SiO_2 beads. The material allows its easy storage (at least, for one year in our experiments) and mixing on demand with different biological substances since all the silver particles are immobilized on the surface of silica microspheres, do not aggregate or change in time, also, the microspheres contain no biologically dangerous substances and are an aseptic product.

Graphene is currently the most intensively studied material for a wide range of applications including electronics, solar energy, batteries and sensors [15]. It is the GO that appears to be a very convenient initial construction block to build up and self-assemble different nanocomposites for a variety of applications, including nanocomposite GO-noble metal nanoparticles [65–71]. The reason to prefer this GO precursor is quite simple and is connected with a possibility to vary physical and chemical properties of GO by simple oxidizing or reducing GO since that brings drastic changes in types and the amount of functional groups and defects associated with GO. Then a strategy, that follows a procedure of GO preparation, includes usually a separate synthesis of noble metal nanoparticles and their binding to the surface of GO using electrostatic forces or chemical interactions with thiols or amines. At the same time, GO itself would be either the reducing and anchoring agent for silver ions therefore Ag@GO nanocomposites benefit these properties. $[Ag(NH_3)_2]^+$ derivatives are suitable precursors for preparation of pure silver nanoparticles thus providing new possibilities

for biocompatible SERS material formation [65]. TEM images showed (Fig. 10l) that the ASP synthesis enables the production of promising Ag@GO nanocomposites with a high silver load, the nanoparticles size of 30–40 nm and a high (about 100 m^2/g) surface area, as optimal for SERS [65].

SERS applications

SERS applications in various fields exploit new possibilities of this method and accumulate new experience in preparation of property-targeted nanomaterials (Table 1). It is important to note that SERS is a nanomaterial-based method that relays on properties dependent on nanostructuring. Therefore nanomaterial preparation methods predetermine, basically, the area of applications of SERS and experimental methods of SERS implementations. All the materials discussed above are probed successfully as SERS active systems for a range of potential analytes like drugs, oil pollutants, biomolecules, cell organelles and intact cells. This evidences for a very universal character of the SERS approach in the modern society and widens perspectives of practical applications of this method and its various modifications in the future. It should be also noted that proper nanocomposite design, such as colloidosomes or smart substrates with nanostructured layers, allows one to achieve a precise combination of functional parameters including biocompatibility, surface area, surface affinity, the number of hot spots and other important optical characteristics providing promising applications of such materials in ecology, biochemistry, medicine, food and oil industries [36].

As a versatile example, silver pseudomorphs demonstrate perspective properties making them favorable for implementation into SERS devices. The octahedral particles produced with the PVP protocol [50] play the role of a highly hierarchic structure being ready for SERS (Fig. 11) of dyes, molecular thiol products and crude

Table 1: Practical applications of SERS-active materials with different morphologies.

SERS material	Preparation features	Physical property features	Application preferences
Hydrosols of isometric nanoparticles	One stage preparation by reduction or self-reduction	A single/narrowed plasmonic peak (with a risk of uncontrolled aggregation of nanoparticles)	Early stage of SERS applications for the limited analysis of biological objects [31–34, 44]
Hydrosols of anisometric nanoparticles	Two stage preparation by seeding and growth	A broad range of plasmon resonance peaks	Application as a precursor for SERS "rainbow" scaffolds for the analysis of biological objects [36, 39, 51]
Pseudomorphic nanoparticles	Topotactic reduction of silver oxide (I) precursor nanoparticles with a given shape	A broad range of plasmon resonance peaks and porous structure with hot spots	Drug and oil molecule analysis [50]
Silica-silver colloidosomes	Heterogeneous seeding and growth	A broad range of plasmon resonance peaks, hot spots and biocompatible surfaces	Intact cell and organelle analysis [35, 36, 39, 41]
Mesoporous silica-silver composites	Heterogeneous seeding and growth or electrostatic attachment of silver nanoparticles	A large surface area combined with capillary condensation, broad effectiveness range of SERS-active nanoparticles	SERS gas sensors [72]
Biocompatible "rainbow" substrates	Deposition of anisometric silver nanoparticle ensemble on biocompatible scaffolds	A broad range of plasmon resonance with a possibility of resonant SERS for a certain fraction of nanoparticles	Intact cell and organelle analysis [36, 39, 51]
Silver ring substrates	Aerosol spray deposition on "warm" substrates	A broad range of plasmon resonance, immobilized nanostructures	Intact cell and organelle and molecular analyte determination [35, 36, 37, 39, 40, 45]
Silver ring substrates coated with "smart" polymers	Aerosol spray deposition on "warm" substrates followed by smart polymer coating	A broad range of plasmon resonance, immobilized nanostructures and preconcentrating/filtering polymer layers	Oil component and molecular analyte determination [36, 37, 42]

oil desulfurization markers in ecology and also for well-known pharmaceutical compounds like meldonium (mildronate, 3-(2,2,2-Trimethyldiazan-2-ium-1-yl)propanoate).

In particular, the SERS spectra of cyclohexanethiol (CHT) represent its adsorbed layers anchored on silver surface by thiol groups. The S-H stretching band usually appearing at 2570 cm^{-1} and also the CSH bending mode at 800–900 cm^{-1} are missing in the SERS spectra showing that the molecules adsorb on the silver surface dissociatively to form a link to silver. In contrast, the 721 cm^{-1} band indicates C-S stretching due to the interaction with silver. Other vibration modes are typical for the cyclohexane ring of its various conformers: ring deformation and stretching at 389 and 845 cm^{-1}, CH_2 twisting, wagging, scissoring and stretching at 1178, 1267, 1363, 1444, 2900 cm^{-1}. Meldonium species can be detected in water at the mM level. Thus, various production protocols of silver pseudomorphs from aqueous diamminesilver (I) hydroxide open up a new effective and simple preparation way of nanostructured particles with desired morphologies for practical applications.

Pyridine is a classical model compound for SERS measurements and it is the very first compound detected by SERS in 1973 after its adsorption onto electrochemically deposited silver [73], also, it is known that affinity of pyridine to silver is high enough and the surface layer seems to be strong due to chemical bonding. The compound demonstrates high delocalization of π electrons and this effect, as well known, increases much the SERS enhancement of such molecules. The pyridine normal modes with the largest Raman intensity are 983 cm^{-1} and 1026 cm^{-1} corresponding to ring breathing; the mode at 598 cm^{-1} is a ring deformation mode; ring stretching modes appear at 1208 cm^{-1}, 1472 cm^{-1} and 1583 cm^{-1}. The most intense peak at 1001 cm^{-1} appear usually in SERS spectra because of a shift by about 20 cm^{-1} due to a chemical interaction with silver surface. Therefore this particular mode could be selected as a reference peak for the estimation of the amount of pyridine. In addition, the boiling point of pyridine at 116 °C favors capillary adsorption. Finally, pyridine is a typical heterocyclic component of crude oil and its content is important to analyze to determine oil quality.

In ref. [72], a gas sensor based on the SERS effect has been developed using silver-silica nanocomposites with mesoporous (MSM-41) SiO_2 possessing a high surface area. The nuclei of silver clusters are distributed homogeneously after the reaction of silica microspheres with hot diamminesilver (I) solutions. Larger silver nanoparticles formed onto microporous silver colloidosomes are attached to the surface. The measured surface area of the mesoporous samples exceeds 1100 cm^2/g and becomes by about 10% higher after the surfactant extraction procedure compared to traditional annealing and therefore the extraction seems to be a predominant technique for creation of open pores [72]. The nanocomposite demonstrates plasmon resonance modes around 400 nm typical of isotropic silver nanoparticles. Such a material is a good candidate for SERS

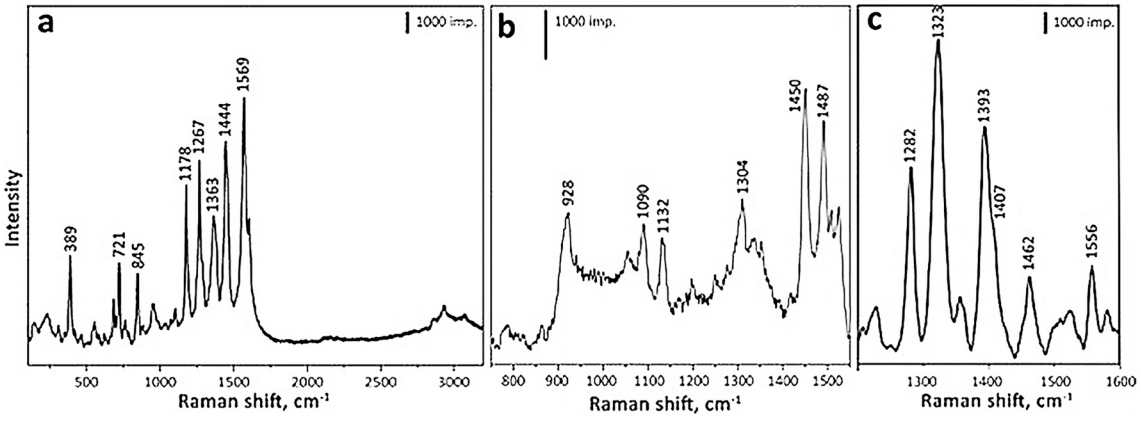

Fig. 11: SERS spectra obtained with silver pseudomorphs of different preparation histories (a, b – pseudomorphic reduction of Ag_2O octahedra with hydrogen peroxide in aqueous ammonia in the presence of PVP, c – ultrasonic spray pyrolysis of aqueous diamminesilver (I) hydroxide): (a) an absorption layer of evaporated CHT (1 mM) measured at 10% of nominal laser power and 10 s of acquisition time, (b) 1 mM concentration of aqueous meldonium, 10% nominal laser power, 60 acquisition time, (c) highly diluted Rhodamine 123 dye of 10^{-10} M concentration.

investigation of gaseous phases and it was used to detect pyridine in vapor at different partial pressures. It was found that there is a distinct correlation between the content of pyridine in vapor and the spectral features of this compound measured using plasmonic nanoparticles of silver decorating mesoporous silica. Mesoporous channels in the colloidosomes favor capillary condensation of organic components of the vapor phase. The detection limit of this compound comprises a better mark that 10–100 ppm. The discussing system is a simpler model example showing a possibility of such an optical analysis near pyridine safety concentration threshold using SERS materials.

The most challenging and pressing problems today are related to environmental issues caused by pollutants originating from oil and oil-derived fuels as the traditional sources of energy. The most common undesirable element in crude oil and its distillates is sulfur, usually ranging in its content from 0.05 to 5% and up to 14% in heavier oil. A mature industrial technology of hydrodesulfurization is effective only for removal of aliphatic sulfur compounds, such as thiols, thioethers and disulfides; however, heterocyclic sulfur compounds, such as thiophene, benzothiophene, dibenzothiophene (DBT) and their alkylated derivatives, cannot be completely removed. Among these, one of the most important markers of fuel quality is 4,6-dimethyldibenzothiophene (4,6-DMDBT), which survives after hydrodesulphurization due to the alkyl groups attached to the ring structure near sulfur because of huge steric hindrance after adsorption on a catalyst surface [36, 37, 74–77]. DBT and its methylated derivatives in fossil fuels are believed to cause acid rains and air pollution; moreover, polycyclic aromatic sulfur heterocyclic (PASH) compounds are widely known to possess biocancerogenic, carcinogenic, mutagenic, and teratogenic properties. Additionally, due to the photodegradation of DBT in water, its oxidized forms such as dibenzothiophene-5,5-dioxide ($DBTO_2$) – which is a patented herbicide – and different alkylated aromatic sulfonic acids – which serve as surfactants – are formed unavoidably leading to the increased toxicity. Thus, DBT with its high toxicity may affect human health and ecosystems [74–77]. Furthermore, fuel sulfur causes in poisoning catalytic converters of vehicles while the stronger environmental standards such as Euro-5 (2011) and ASTM (2015) require stricter control over pollutants. The maximum permissible level of sulfur content in diesel fuels in Europe and USA is currently 10 and 1 ppm, respectively, with targets of zero emissions. The new environmental regulations promoted studies of alternative technologies to purify fuels like catalytic oxidative desulfurization. Practically, these regulations mean that impurity-level concentrations of DBTs and DBTO/$DBTO_2$ should be measured and therefore preconcentration has to be employed in order to increase analytical signals, especially in the case of oxidized forms of DBTs [36].

SERS becomes one of the most interesting and promising techniques towards direct ultrasensitive detection of various analytes in complex samples [36, 37, 78–81]. Some successful attempts are known to apply SERS for non-polar chemical pollutants such as polycyclic aromatic hydrocarbons (PAHs) at low concentration [37, 78–81]. An optimum tuning of chemical properties of the nanostructured substrates may lead to their higher affinities toward certain classes of analytes. Polymer thin layers can be used to tune SERS efficiency and obtain optimal conditions for better enhancement factors [37]. This innovative idea to detect and quantify sulfur-organic molecules in oil and environment by SERS can be readily implemented using easy-to-prepare active elements of optical sensors with no need of complex sample preparation steps. A new concept of preconcentration, recognition, binding, and optical properties adjustment of analytes using planar optical sensors is based on nanostructured silver substrates coated with a thin layer of optically transparent chitosan gel [37]. The unique features of the proposed approach consist in registration of highly enhanced signal of charge-transfer complexes (CTCs) formed in a thin layer of polymer chemically modified by a π-acceptor that is capable of recognizing important analytes by binding with them in CTC thus providing the detection of individual PASH compounds as new electronic-vibrational structures that can be seen in resonant Raman scattering spectra [37, 81].

All sulfur organic polycyclic pollutants – DBT, 4,6-DMDBT, DBTO and $DBTO_2$ – absorb UV at 230–290 nm but have no strong absorption modes in a visual light range, they alone demonstrate weak enhancement in SERS spectra. DBT can act both as an n type donor by the lone pair of the sulfur atom or as a π type donor by the delocalized electrons of the aromatic rings. Formation of CTC is generally accompanied by the appearance of a new absorption Benesi Hildebrand bands. The formed CTCs provide light absorption in the 500–650 nm range

thus giving the possibility to agitate their electronic structure by standard 514 and/or 633 nm lasers typically used for RSS; in accordance with our data, 7,7,8,8-tetracyanoquinodimethane (TCNQ), and 2,3-dichloro-5,6-dicyanobenzoquinone (DDQ) are effective as suitable π acceptors [36, 37, 81].

In general, such CTC can be successfully involved within a universal approach of detection of important analytes like nonpolar organic molecules thus expanding the suggested approach toward environmental control of water, air, soil and quality control of fuel (Fig. 12) [36, 37, 81]. Despite of the key importance of the silver nanostructured layer, it should be coated by a microporous polymer film with thickness of 5–10 μm which is chemically modified with acceptor compounds ensuring the generation of bright SERS signals from the targeted analytes. Such newly proposed microporous optically transparent polymer layer acts as a protective coating and, simultaneously, as an effective absorbent of PASHs. Another important role of the polymer consists in trapping of the analytes. Chitosan films on the glass were transparent, very flexible and had smooth surfaces. As CS is a linear polysaccharide composed of randomly distributed deacetylated and acetylated D-glucosamine units, it may hold in its structure a solvent and the dissolved molecules thus preconcentrating them. The presence of both amino and hydroxyl groups in CS monomers causes excellent chelating and film-forming properties. Due to the effect of molecular sieves and hydrophobic interactions, CS could capture various compounds from nonpolar solvents such as saturated hydrocarbons. At the same time the CS layer affects no silver nanostructures. The developed method makes it possible to control quantitative yields of catalytic oil desulfurization processes with a necessary accuracy and precision as well as to determine the purity of industrial fuel and concentration of environmental pollutants. This indicator system based on trapping analytes within colored CTCs allows a multiplex analysis of PASHs due to significant differences in the Raman spectra of the analytes with different molecular structures. Selectivity and stability of the analysis are provided by a correct choice of appropriate π-acceptors which are immobilized within the polymer layer. The suggested strategy of express diagnostics of fuels and environmental health opens new frontiers toward applications of SERS [36, 37].

Recent trends of SERS applications consider an enhancement of Raman scattering of molecules separated from nanoparticles by a certain structure (for example, cell membranes, Fig. 13), that is highly demanded for studies of biomolecules in their natural environment in cells or organelles [34–36, 38, 39, 41, 45, 51]. If the nanoparticles are free and surrounded by electrolytes, they might aggregate and be stuck onto the surface of cells. Our results demonstrate that even small silver nanoparticles themselves are not damaging objects for the erythrocytes, at least in terms of mechanical destruction of the membranes and pronounced chemical interactions with lipids (Fig. 13). It is important to understand that, in the case of single molecules, the enhancement of Raman signal occurs due to, at least, several known reasons, including a local electrical field

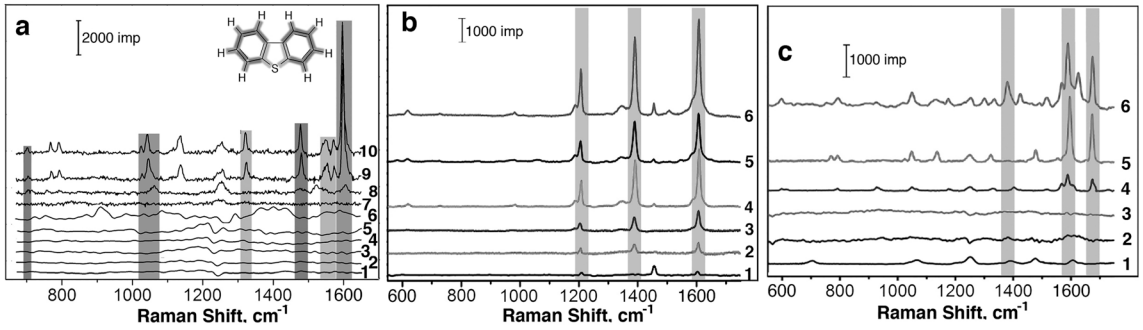

Fig. 12: RS and SERS spectra of (a) polymer layers on the nanostructured silver ring layer: pure glass (for comparison) (1), HEC (hydroxyethylcellulose) (2), PVP (polyvinylpyrrolidone) (3), PVA (polyvinylalcohol) (4), CS (chytosan) (5) coatings and 6- the same with 5-fold increased thickness (RS spectra were measured using power neutral density filter 50%). SERS/resonant SERS of charge transfer complex DBT-DDQ on the silver rings with (a) PVP (7), PVA (8), CS (9), HEC (10); (b) with TCNQ (0.5 mM), no analyte (1), DBT (2), 4,6-DMDBT (3), charge-transfer complexe (CTC) with $DBTO_2$ (4), CTC with model mixture DBT:4,6-DMDBT:DBTO (1:10:9) (5), CTC with DBTO (6) and (c) with DDQ (5 mM), no analyte (1), $DBTO_2$ (2), DBTO (3), CTC with 4,6-DMDBT (4), CTC with DBT (5), CTC with a model mixture of DBT:4,6-DMDBT:DBTO (1:10:9) (6).

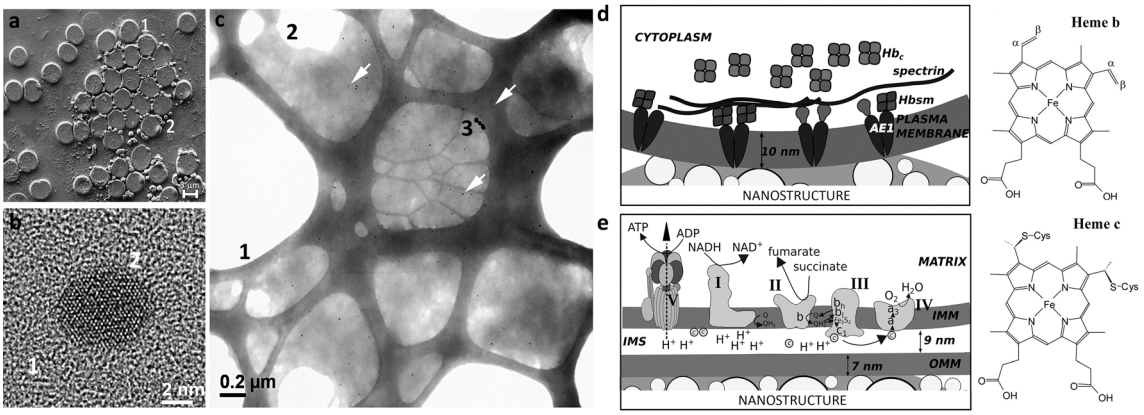

Fig. 13: Interaction of silver nanoparticles with erythrocyte membranes. (a) a general SEM view of erythrocytes mixed with silver hydrosol, (b) a TEM image of a part of erythrocyte membrane (1) with a small silver nanoparticle (2), (c) a general view of erythrocyte ghosts (vesicles of erythrocyte membranes) mixed with silver hydrosol, "1" marks an edge of TEM mesh, "2" corresponds to the edge of erythrocyte membrane (host), "3" – large silver nanoparticles onto the membrane, smaller AgNPs are marked with the arrows. (d, e) cells and cells organelles studied by SERS; (d) a scheme of a submembrane region of an erythrocyte contacting with colloidosomes and a 10 nm thick cell membrane. Hbsm, Hbc – molecules of the submembrane and cytosolic hemoglobin (Hb), respectively; (e) a scheme of outer and inner mitochondrial membranes (OMM and IMM, respectively) with the complexes I–V of the electron transport chain (ETC). The cytochrome *c* is shown as balls diffusing in the intermembrane space (IMS).

amplification, a charge transfer between nanoparticles and the molecules and because of the "hot spot" formation. It is commonly considered that intense SERS spectra with well-defined peaks can be observed mostly for molecules that are attached to plasmonic nanostructures. However molecules inside living cells have no physical contacts with nanoparticles. Obviously, that the "hot spot" and the charge transfer enhancement both vanish in this particular case since they, indeed, require such a contact. Therefore the remaining electromagnetic field enhancement becomes the dominant mechanism predetermined by morphological features of the nanostructured surface.

SERS combines molecular fingerprint specificity and, potentially, single-molecule sensitivity. Simple easy-to-prepare sols of noble metal nanoparticles are the most popular and widespread in SERS investigations. However, despite of all possible advantages, the nanoparticles themselves are likely to aggregate uncontrollably in solutions making it difficult to reproduce SERS results. The most important tasks of modern medicine are related to prognostics, early diagnosis and timely complex therapy of socially significant diseases. This creates new requirements for establishing of the concentrations, conformations and activity of chromoproteins, their complexes with biologically active compounds, studying the kinetics of metabolite formation during the functioning of intact cells and cell organelles, which, in turn, necessitates the development of new approaches and tools for analyzing functioning in living tissue structures. It is important to note that laser excitation wavelengths for SERS can be used, in the case of wide spread porphyrin biosystems, in the regions of Soret and beta-bands (for example, with 404, 417 or 532 nm lasers, see Fig. 5d) making it possible to achieve the resonant Raman amplification.

Such conditions favor a much higher enhancement of Raman scattering signal of the analyte if plasmonic nanostructures also absorb light in the same regions. The violet laser irradiation fits well either the most bright Soret absorption band or the typical plasmon resonance position of spherical silver nanoparticles. Unfortunately this wavelength damages biological objects, and is still exotic; also, it is almost impossible to keep single silver nanoparticles separated in chloride salines therefore, it is a usual route in many SERS experiments with biological objects to prepare artificially colloidal aggregates with their absorption shifted up to "green lasers" as achieved by their intentional "activation" in sodium chloride solutions. Nanoparticle sols exhibit also limited plasmonic tuneability as compared to colloidosomes or silver-ring substrates. This leads to the

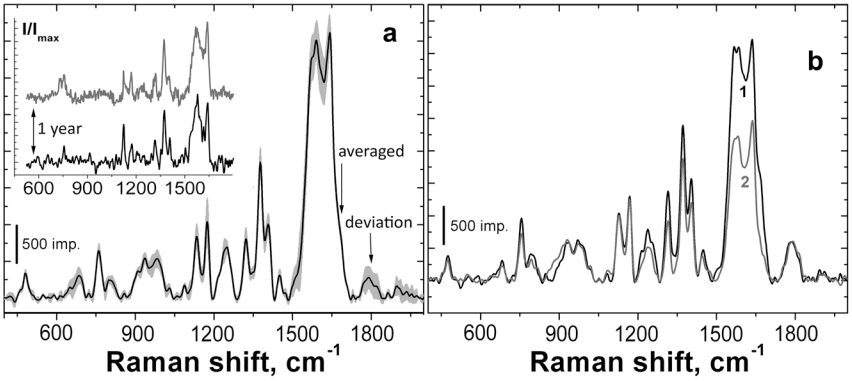

Fig. 14: Reproducibility of SERS spectra of functioning mitochondria using Ag@SiO_2 colloidosomes: (a) averaged spectrum (thick black line) and standard deviations (gray area) for a series of spectra measured from either one and the same or different points. The inset shown two spectra measured using the same colloidosomal material but for different mitochondria series with a period of separate measurements of about one year, (b) SERS spectra of mitochondria with (1) or without (2) addition of a substrates for ATP synthesis and electron donors for ETC (ADP (0.1 mM), $MgCl_2$ (2 mM), pyruvate (2 mM), malate 2 mM), succinate (5 mM).

approach based on preparation of "rainbow substrates", as described above, or the application of hierarchic nanostructured silver materials providing absorption in a wide spectral range.

The colloidosome family of SERS nanocomposites, with hybridization of plasmon modes supported by an inner cavity and an outer surface of the nanoshell, allows to tune plasmon resonance bands readily by the size of the cores, the thickness of the metal shells, the dielectric core coverage with plasmonic nanoparticles and the coupling between neighboring particles. A great enhancement of Raman scattering (SERS) from heme-containing submembrane biomolecules inside intact erythrocytes and functional mitochondria is demonstrated most effectively using either the silver ring substrates or silver-silica beads prepared by the method of aerosol pyrolysis with aqueous diamminesilver (I) hydroxide as a unique source of plasmonic nanoparticles for SiO_2 microspheres [35, 41, 45, 51].

The recorded SERS spectra (Fig. 14) reveal a set of characteristic peaks at 750, 1127, 1170, 1371, 1565, 1585 and 1638 cm^{-1} resulting from the normal group vibrations of pyrrol rings, methine bridges and side radicals in the heme molecules [35, 36, 39, 41]. Mitochondria are organelles of fundamental importance for cellular energy production, metabolic regulation, aging and cell survival under stress. Normal function of mitochondria and their pathological changes, including production of reactive oxygen species (ROS), are heavily dependent on the redox state of the electron transport chain (ETC) cytochromes and cytochrome *c*, in particular. The direct information about the cytochrome *c* redox state and its intermembrane space (IMS) dynamics in living mitochondria is still difficult to obtain since the redox state and the conformation of cytochrome *c* are highly dynamic, affecting its diffusion in IMS, interaction with complexes III and IV and the electron transfer (see Fig. 13d and e). Thus, sensitive, noninvasive, label-free analysis of cytochrome *c* inside intact functional mitochondria can extend our understanding of cytochrome *c* role in the modulation of the ETC activity and development of mitochondria pathologies. A selective study of the ETC components in living mitochondria is essential for fundamental biophysical research and for the development of new medical diagnostic methods. However, many important details of inter- and intramembrane mitochondrial processes have remained in shadow due to the lack of non-invasive techniques. The SERS spectra of functional mitochondria are found to be sensitive to the activity of the mitochondrial ETC thus making the SERS method a novel label-free approach to monitor the redox state and conformation of cytochromes in their natural cell environment [35, 41]. The discussed nanocomposites are highly suitable for the analysis of biological objects due to their robust prepared scheme, superior spatial and temporal signal reproducibility preserved for a period of at least one year (Fig. 14), this would lead to the development of new express systems with record sensitivity and specificity in the interests of medical screening and personal medicine.

Conclusions

Silver is seen to be a unique chemical element, which allows production by simple routes of a great variety of diverse nanoparticles and nanostructures. This feature opens up new important possibilities of either increasing spectral and concentration sensitivity or increasing specificity of SERS based sensors with foreseeable applications in the fields of medicine, health, ecology and advanced fuel analysis thus making silver one of the most important "nanoelements" of the Dmitry Mendeleev's Periodic Table.

Acknowledgments: The authors are grateful to V.K.Ivanov. A.E.Barantchikov, S.V.Savilov, E.I.Nikelshparg, G.V.Maximov for fruitful discussions.
Funding: IAV thanks the Russian Science Foundation for support (grant 19-13-00283).

References

[1] E. Fermi. *Z. Phys.* **48**, 73–79 (1928).
[2] Y. D. Tretyakov, E. A. Goodilin. *Russ. Chem. Rev.* **78**, 801–820 (2009).
[3] D. A. Tomalia, S .N. Khanna. *Chem. Rev.* **116**, 2705–2774 (2016).
[4] E. A. Goodilin, P. S. Weiss, Y. Gogotsi. *ACS Nano* **13**, 10879–10886 (2019).
[5] T. Radford. *Nature* **565**, 564–565 (2019).
[6] P. Ball. *Nature* **565**, 552–555 (2019).
[7] J. Rampling. *Nature* **565**, 563–564 (2019).
[8] M. Poliakoff, A. D. Makin, S. L. Y. Tang, E. Poliakoff. *Nat. Chem.* **11**, 391–393 (2019).
[9] A. A. Semenova, A. B. Tarasov, E. A. Goodilin. *Mendeleev Commun.* **29**, 479–485 (2019).
[10] E. R. Scerri. *Chem.: Eur. J.* **25**, 7410–7415 (2019).
[11] C. Balarew. *Pure Appl. Chem.* **91**, 2037–2042 (2019).
[12] P. Simon, Y. Gogotsi. *Nat. Mater.* **7**, 845–854 (2008).
[13] T. K. Zakharchenko, A. Y. Kozmenkova, D. M. Itkis, E. A. Goodilin. *Beilstein J. Nanotechnol.* **4**, 758–762 (2013).
[14] D. Golberg, Y. Bando, Y. Huang, T. Terao, M. Mitome, C. C. Tang, C. Y. Zhi. *ACS Nano* **4**, 2979–2993 (2010).
[15] K. S. Novoselov, D. Jiang, F. Schedin, T. J. Booth, V. V. Khotkevich, S. V. Morozov, A. K. Geim. *Proc. Natl. Acad. Sci. USA* **102**, 10451–10453 (2005).
[16] M. Naguib, Y. Gogotsi. *Acc. Chem. Res.* **48**, 128–135 (2015).
[17] V. A. Krivchenko, D. M. Itkis, S. A. Evlashin, D. A. Semenenko, E. A. Goodilin, A. T. Rakhimov, A. S. Stepanov, N. V. Suetin, A. A. Pilevsky, P. V. Voronin. *Carbon* **50**, 1438–1442 (2012).
[18] M. Bruchez, M. Moronne, P. Gin, S. Weiss, A. P. Alivisatos. *Science* **281**, 2013–2016 (1998).
[19] P. Tiwana, P. Docampo, M. B. Johnston, H. J. Snaith, L. M. Herz. *ACS Nano* **5**, 5158–516 (2011).
[20] I. Turkevych, S. Kazaoui, N. A. Belich, A. Y. Grishko, S. A. Fateev, A. A. Petrov, T. Urano, S. Aramaki, S. Kosar, M. Kondo, E. A. Goodilin, M. Graetzel, A. B. Tarasov. *Nat. Nanotechnol.* **14**, 57–63 (2019).
[21] A.A. Petrov, I. P. Sokolova, N. A. Belich, G. S. Peters, P. V. Dorovatovskii, Y. V. Zubavichus, V. N. Khrustalev, A. V. Petrov, M. Gratzel, E. A. Goodilin, A. B. Tarasov. *J. Phys. Chem. C.* **121**, 20739–20743 (2017).
[22] M. Haase, H. Schafer. *Angew. Chem., Int. Ed.* **50**, 5808–5829 (2011).
[23] A. H. Lu, E. L. Salabas, F. Schuth. *Angew. Chem., Int. Ed.* **46**, 1222–1244 (2007).
[24] E .A. Goodilin, E. A. Pomerantseva, V. V. Krivetsky, D. M. Itkis, J. Hester, Y. D. Tretyakov. *J. Mater. Chem.* **15**, 1614–1620 (2005).
[25] E. A. Pomerantseva, D. M. Itkis, E. A. Goodilin, J. G. Noudem, M. V. Lobanov, M. Greenblatt, Y. D. Tretyakov. *J. Mater. Chem.* **14**, 1150–1156 (2004).
[26] M. Chhowalla, H. S. Shin, G. Eda, L. J. Li, K. P. Loh, H. Zhang. *Nat. Chem.* **5**, 263–275 (2013).
[27] R. Z. Valiev, R. K. Islamgaliev, I. V. Alexandrov. *Prog. Mater. Sci.* **45**, 103–189 (2000).
[28] A. Y. Polyakov, A. Zak, R. Tenne, E. A. Goodilin, K. A. Solntsev. *Russ. Chem. Rev.* **87**, 251–271 (2018).
[29] K. A. Willets, R. P. Van Duyne. *Annu. Rev. Phys. Chem.* **58**, 267–297 (2007).
[30] P. K. Jain, X. H. Huang, I. H. El-Sayed, M. A. El-Sayed. *Acc. Chem. Res.* **41**, 1578–1586 (2008).
[31] S. M. Nie, S. R. Emery. *Science* **275**, 1102–1006 (1997).
[32] Y. G. Sun, Y. N. Xia. *Science* **298**, 2176–2179 (2002).
[33] N. L. Rosi, C. A. Mirkin. *Chem. Rev.* **105**, 1547–1562 (2005).
[34] N.A. Brazhe, E. Y. Parshina, V. V. Khabatova, A. A. Semenova, A. R. Brazhe, A. I. Yusipovich, A. S. Sarycheva, A. A. Churin, E. A. Goodilin, G. V. Maksimov, O. V. Sosnovtseva. *J. Raman Spectrosc.* **44**, 686–694 (2013).

[35] N. A. Brazhe, A. B. Evlyukhin, E. A. Goodilin, A. A. Semenova, S. M. Novikov, S. I. Bozhevolnyi, B. N. Chichkov, A. S. Sarycheva, A. A. Baizhumanov, E. I. Nikelshparg, L. I. Deev, E. G. Maksimov, G. V. Maksimov, O. Sosnovtseva. *Sci. Rep.* **5**, srep13793-1–13 (2015).
[36] O. E. Eremina, A. A. Semenova, E. A. Sergeeva, N. A. Brazhe, G. V. Maksimov, T. N. Shekhovtsova, E. A. Goodilin, I. A. Veselova. *Russ. Chem. Rev.* **87**, 741–770 (2018).
[37] O. E. Eremina, A. V. Sidorov, T. N. Shekhovtsova, E. A. Goodilin, I. A. Veselova (2017). *ACS Appl. Mater. Interfaces* **9**, 15058–15067.
[38] E. Y. Parshina, A. S. Sarycheva, A. I. Yusipovich, N. A. Brazhe, E. A. Goodilin, G. V. Maksimov. *Laser Phys. Lett.* **10**, 075607-1–6 (2013).
[39] A. A. Semenova, A. P. Semenov, E. A. Gudilina, G. T. Sinyukova, N. A. Brazhe, G. V. Maksimov, E. A. Goodilin. *Mendeleev Commun.* **26**, 177–186 (2016).
[40] A. S. Sarycheva, A. A. Semenova, E. Y. Parshina, N. A. Brazhe, A. Y. Polyakov, A. Y. Kozmenkova, A. V. Grigorieva, G. V. Maksimov, E. A. Goodilin. *Mater. Lett.* **121**, 66–69 (2014).
[41] A. S. Sarycheva, N. A. Brazhe, A. A. Baizhumanov, E. I. Nikelshparg, A. A. Semenova, A. V. Garshev, A. E. Baranchikov, V. K. Ivanov, G. V. Maksimov, O. V. Sosnovtseva, E. A. Goodilin. *J. Mater. Chem. B.* **3**, 539–546 (2016).
[42] A. S. Sarycheva, V. K. Ivanov, A. E. Baranchikov, S. V. Savilov, A. V. Sidorov, E. A. Goodilin. *RSC Adv* **5**, 90335–90342 (2015).
[43] A. A. Semenova, V. K. Ivanov, S. V. Savilov, E. A. Goodilin. *CrystEngComm.* **15**, 7863–7871 (2013).
[44] A. A. Semenova, N. A. Brazhe, E. Y. Parshina, V. K. Ivanov, G. V. Maksimov, E. A. Goodilin. *Plasmonics* **9**, 227–235 (2014).
[45] A. A. Semenova, E. A. Goodilin, N. A. Brazhe, V. K. Ivanov, A. E. Baranchikov, V. A. Lebedev, A. E. Goldt, O. V. Sosnovtseva, S. V. Savilov, A. V. Egorov, A. R. Brazhe, E. Y. Parshina, O. G. Luneva, G. V. Maksimov, Y. D. Tretyakov. *J. Mater. Chem.* **22**, 24530–24544 (2012).
[46] C. A. Mirkin, R. L. Letsinger, R. C. Mucic, J. J. Storhoff. *Nature* **382**, 607–609 (1996).
[47] Y. N. Xia, G. M. Whitesides. *Annu. Rev. Mater. Sci.* **28**, 153–184 (1998).
[48] X. H. Huang, I. H. El-Sayed, W. Qian, M. A. El-Sayed. *J. Am. Chem. Soc.* **128**, 2115–2120 (2006).
[49] J. Fang, S. Liu, Z. Li. *Biomaterials* **32**, 4877–4884 (2011).
[50] A. A. Semenova, S. V. Savilov, A. E. Baranchikov, V. K. Ivanov, E. A. Goodilin. *Mendeleev Commun.* **29**, 395–397 (2019).
[51] A. A. Semenova, N. A. Brazhe, E. Y. Parshina, A. S. Sarycheva, G. V. Maksimov, E. A. Goodilin. *RSC Adv* **6**, 85156–85164 (2016).
[52] I. Pastoriza-Santos, L. M. Liz-Marzan. *J. Mater. Chem.* **18**, 1724–1737 (2008).
[53] T. Huang, X. H. N. Xu. *J. Mater. Chem.* **20**, 9867–9876 (2010).
[54] X. Y. Zhang, A. Hu, T. Zhang, W. Lei, X. J. Xue, Y. Zhou, W. W. Duley. *ACS Nano* **5**, 9082–9092 (2011).
[55] B. Pietrobon, V. Kitaev. *Chem. Mater.* **20**, 5186–5190 (2008).
[56] D. E. Charles, D. Aherne, M. Gara, D. M. Ledwith, Y. K. Gun'ko, J. M. Kelly, W. J. Blau, M. E. Brennan-Fournet. *ACS Nano* **4**. 55–64 (2010).
[57] J. Zeng, X. Xia, M. Rycenga, P. Henneghan, Q. Li, Y. Xia. *Angew. Chem. Int. Ed.* **50**, 244–249 (2011).
[58] N. Cathcart, A. J. Frank, V. Kitaev. *Chem. Commun.* **46**, 7170–7172 (2009).
[59] S. Coskun, B. Aksoy, H. E. Unalan. *Cryst. Growth Des.* **11**, 4963–4969 (2011).
[60] A. A. Semenova, V. K. Ivanov, A. E. Baranchikov, S. V. Savilov, E. A. Goodilin. *Funct. Mater. Lett.* **9**, 1650014-1–4 (2016).
[61] W. Stöber, A. Fink, E. Bohn. *J. Colloid Interface Sci.* **26**, 62–69 (1968).
[62] X. H. Liu, Y. Y. Cao, H. Y. Peng, H. S. Qian, X. Z. Yang, H. B. Zhang. *CrystEngComm.* **16**, 2365–2370 (2014).
[63] K. Wang, X. Zhang, C. Niu, Y. Wang. *ACS Appl. Mater. Interfaces* **6**, 1272–1278 (2014).
[64] T. Liu, D. Li, D. Yang, M. Jiang. *Colloids Surf. A.* **387**, 17–22 (2011).
[65] M. O. Volodina, A. Y. Polyakov, A. V. Sidorov, A. V. Grigorieva, E. A. Eremina, S. V. Savilov, E. A. Goodilin. *Mendeleev Commun.* **26**, 231–234 (2016).
[66] W. Ren, Y. Fang, E. Wang. *ACS Nano* **5**, 6425–6433 (2011).
[67] V. K. Gupta, N. Atar, M. L. Yola, M. Eryilmaz, H. Torul, U. Tamer, I. H. Boyaci, Z. Ustundag. *J. Colloid Interface Sci.* **406**, 231–237 (2013).
[68] X. Liu, L. Cao, W. Song, K. Ai, L. Lu. *ACS Appl. Mater. Interfaces* **3**, 2944–2952 (2011).
[69] H. D. Jang, S. K. Kim, H. Chang, J. W. Choi. *Biosens. Bioelectron.* **63**, 546–551 (2015).
[70] L. Li, B. An, A. Lahiri, P. Wang, Y. Fang. *Carbon* **65**, 359–364 (2013).
[71] G. Goncalves, P. A. A. P. Marques, C. M. Granadeiro, H. I. S. Nogueira, M. K. Singh, J. Gracio. *Chem. Mater.* **21**, 4796–4802 (2009).
[72] A. S. Sarycheva, A. A. Semenova, E. A. Goodilin. *Nanosystems: Phys. Chem. Math.* **8**, 579–585 (2017).
[73] M. Fleishmann, P. J. Hendra, A. J. McQuillan. *Chem. Phys. Lett.* **26**, 163–166 (1974).
[74] M. V. Landau, D. Berger, M. Herskowitz. *J. Catal.* **159**, 236–245 (1996).
[75] J. T. Andersson. *Chemosphere* **27**, 2097–2102 (1993).
[76] K. G. Kropp, P. M. Fedorak. *Can. J. Microbiol.* **44**, 605–622 (1998).
[77] I. V. Babich, J. A. Moulijin. *Fuel* **82**, 607–631 (2003).
[78] R. A. Alvarez-Puebla, L. M. Liz-Marzan. *Energy Environ. Sci.* **3**, 1011–1017 (2010).

[79] P. Leyton, S. Sanchez-Cortez, J. V. Garcia-Ramos, C. Domingo, M. Campos-Vallette, C. Saitz, R. E. Clavijo. *J. Phys. Chem. B.* **108**, 17484–17490 (2004).
[80] L. Guerrini, J. Garsia-Ramos, C. Domingo, S. Sanchez-Cortes. *Phys. Chem. Phys.* **11**, 1787–1793 (2009).
[81] A. V. Sidorov, O. E. Vashkinskaya, A. V. Grigorieva, T. N. Shekhovtsova, I. A. Veselova, E. A. Goodilin. *Chem. Commun.* **50**, 6468–6470 (2014).